PRECISION INSERTION DEVICE CONTROL AND SIMULTANEOUS MONOCHROMATOR FLY SCANNING FOR NSLS-II

J. Sinsheimer*, P. Louis Cappadoro, T. Corwin, J. Escallier, D. Harder, D. A. Hidas,
A. Hunt, M. Musardo, J. Rank, C. Rhein, T. Tanabe, I. Waluyo
Brookhaven National Laboratory, Upton, USA

Abstract

Beginning in January of 2019, 8 of the 10 In-Vacuum Undulators installed in the NSLS-II storage ring underwent in-house in-situ control system upgrades allowing for control of the magnetic gap during motion down to the 50 nm level with an in-position accuracy of nearly 5 nm. Direct linking of Insertion Devices and beamline monochromators is achieved via a fiber interface allowing precise, simultaneous, nonlinear motion of both devices and providing a fast hardware trigger for real-time accurate insertion device and monochromator fly scanning. This presentation will discuss use case scenarios at light source facilities and detail the precision achieved for simultaneous motion. Particular attention is given to the precision at which undulator energy harmonic peaks can be tracked and the variation of the peak flux in motion.

INTRODUCTION

Between January and April of 2019, eight of the 10 In-Vacuum Undulators (IVUs) installed in the NSLS-II storage ring underwent in-house in-situ control system development and replacement. The motivation for this was to correct the underperforming and unreliable operation of the vendor supplied systems, speed up step-scanning, and lay the proper groundwork for Insertion Device (ID) and monochromator synchronization for fast fly scanning of photon energy while maintaining peak photon flux. Step scanning speeds were improved by a factor of nearly five and all eight IVUs are currently running with extremely high reliability. The first real-time synchronization of an ID and monochromator has been achieved with one of the out-of-vacuum Elliptically Polarizing Undulators (EPUs) for the In situ and Operando Soft X-ray Spectroscopy (IOS) beamline with another IVU and EPU to follow shortly.

IVU CONTROL SYSTEMS UPGRADE

The eight IVUs that underwent a complete software overhaul are three 2.8 [m] long 23 [mm] period (IVU23), three 1.5 [m] long 21 [mm] period (IVU21), and two 3 [m] long 20 [mm] period (IVU20) devices. The simplest with regard to the control system among them are the two IVU20s which have one motor to control the magnetic gap and one for device elevation. This type device will not be discussed in detail, but can be thought of as the single-axis (gap) analog of the more complicated systems discussed herein. The remaining six IVUs (IVU21s and IVU23s) each have four
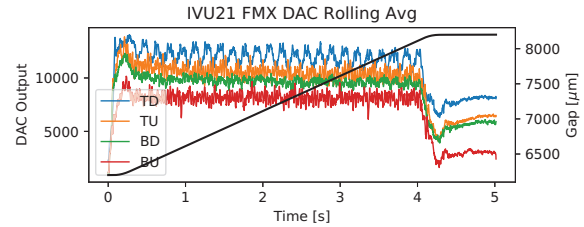
_____

* jsinsheimer@bnl.gov

Figure 1: DAC output rolling average showing output during motion for each motor with notable oscillatory behavior of the TD output possibly indicating component misalignment or wear as an example of diagnostic plots used at NSLSII.

motor axes which we denote TU, TD, BU, and BD (where: T - Top, B - Bottom, U - Upstream, D - Downstream). The simple linear transformation shown in Eq. (1) gives the useful coordinates of gap, elevation, taper, and tilt of the device. This transformation and its inverse are used to form the forward and inverse kinematics for device motion. The IVU21 devices have an additional jack elevation motor axis which is used for alignment and not used in normal operation which is of little interest here and not discussed further.

The DeltaTau Brick Controller is used for motion control. Renishaw 1 [nm] linear encoders are used for position feedback on the four girder gap axes while the rear mounted motor rotary encoders are used for velocity feedback. Proportional Integral Derivative (PID) tuning is performed separately for top-girder and bottom-girder drives. The DeltaTau drives external servo amplifiers with a ± 10 [V] analog signal (here referred to as DAC output). It is noted here that from this output one may glean insight into mechanical misalignment or wearing, possibly preventing damage or failure if monitored occasionally. An example of this this is shown in Fig. 1. It is also noted that in these systems the linear encoders are not mounted in line with the drive shafts and may suffer from a dual feedback cantilever resonance effect. This effect has been witnessed in less massive devices [1].

$$\begin{bmatrix} gap \\ elevation \\ taper \\ tilt \end{bmatrix} = \begin{bmatrix} \frac{1}{2} & \frac{1}{2} & \frac{1}{2} & \frac{1}{2} \\ \frac{1}{4} & \frac{1}{4} & -\frac{1}{4} & -\frac{1}{4} \\ 1 & -1 & 1 & -1 \\ \frac{1}{2} & -\frac{1}{2} & -\frac{1}{2} & \frac{1}{2} \end{bmatrix} \begin{bmatrix} TU \\ TD \\ BU \\ BD \end{bmatrix} \quad (1)$$

IVU CONTROL PERFORMANCE

It is highly desirable to have well behaved ID gap movement during operations, not only as a prerequisite to simultaneous ID-monochromator scanning, but also to minimize

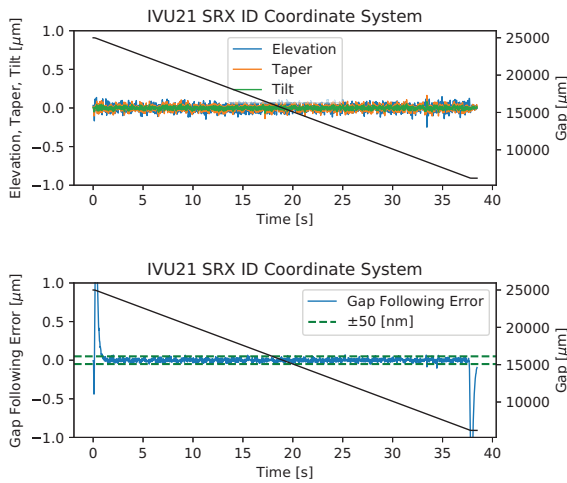**Device Control and Integrating Diverse Systems**

Figure 2: Top: Elevation, Taper, and Tilt during gap motion shown for completeness. Bot: Gap error during full range motion shown to be within 50 [nm].
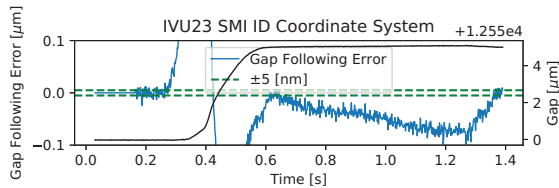

Figure 3: Gap motion for a five micrometer gap move showing gap error at beginning and end of movement is nearly within five nanometers (at the scale) for one of the large IVU23 device.

any effect on the electron beam that would which would normally be compensated by an active feed-forward corrector system which typically utilize the gap readback value. In this case it is sensible to ensure that the elevation, taper, and tilt are also well behaved during motion which can be seen for the one of the IVU21 devices in top of Fig. 2. During motion of these devices the gap is particularly well behaved with the typical following errors (commanded minus actual) during motion in the range of ±50 [nm] as can be see in the bottom plot of Fig. 2. Note that at the beginning and end of motion the following error peaks, which is expected because of high inertial loads, but it is symmetric such that the gap itself is smooth with minimal disturbance of the elevation, taper, and tilt.

The final settling gap value precision is almost five nanometers as can be see on the left and right side of Fig. 3 where the gap and following error is shown for a fairly quick five micrometer gap change.

ID MONOCHROMATOR FLY SCAN

Beamline capabilities can be improved through synchronized motion of the ID and monochromator for fast scanning in energy where the output flux of the ID is maximized in line with the monochromator energy. This has previously
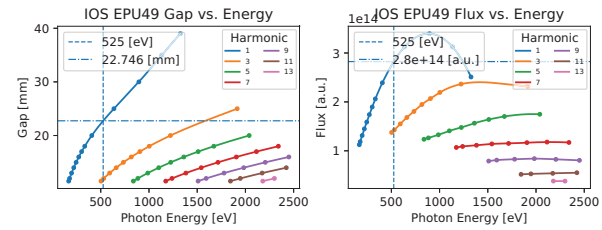

Figure 4: Lookup tables for magnetic gap, photon energy, and photon flux are calculated from magnetic field data acquired from the NSLSII magnetic measurement laboratory.
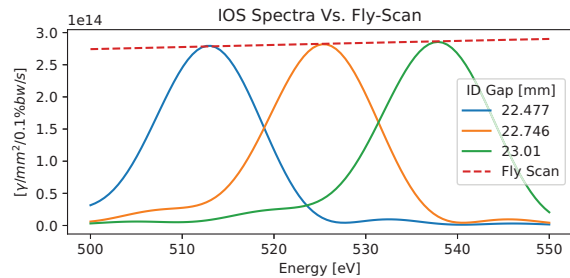

Figure 5: A comparison of the flux of the stationary state spectra at different gaps to the ideal flux from synchronized ID-monochromator fly scan motion.

been done in a quasi-synchronous fashion utilizing network interfaces, which are prone to latency and typically do not deliver real-time feedback [2]. The solution applied at NSLSII utilizes the DeltaTau MACRO fiber interface between the two controllers allowing real-time control of both the ID and monochromator. Both the ID and monochromator are incorporated into a single coordinate system with full forward and reverse kinematics defined for the combined system. Once this is in place one only needs to have knowledge of the gap for a given photon energy on a given undulator harmonic. These tables can be calculated theoretically [3] from magnetic field data collected in the NSLSII magnetic measurement laboratory [4, 5] as is shown for the IOS device in Fig. 4. In practice these curves are also calculated from measured spectra at the beamline. These curves are needed due to the gap motion not being linearly correlated with the photon energy peak.

Figure 5 shows an example of a theoretical fly scan from 500 to 550 [eV] and how the flux varies along the fly scan as compared with the spectra of 3 intermediate stationary gap values along the scan trajectory. It is noted here that it is also possible to construct a scan where the flux is constant by offsetting the gap value at different energies, but one should take into account photon polarization effects if high precision is required.

Position measurements from a test scan (recorded real-time within controller hardware) are summarized in Fig. 6 which shows the ID gap, plane grating monochromator (PGM), and following errors for each. Two things of note are that the accuracy of the ID control can be improved using the
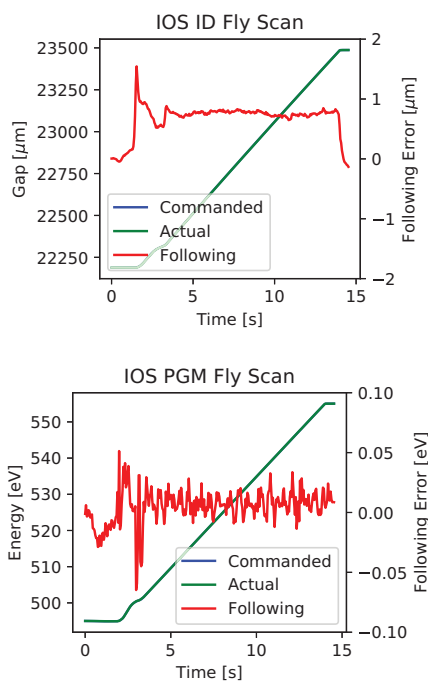
Figure 6: Data collected from a fly scan with ID and monochromator motion synchronized. The top plot shows the gap motion and following error while the bottom shows PGM energy and energy deviation from the ideal trajectory.
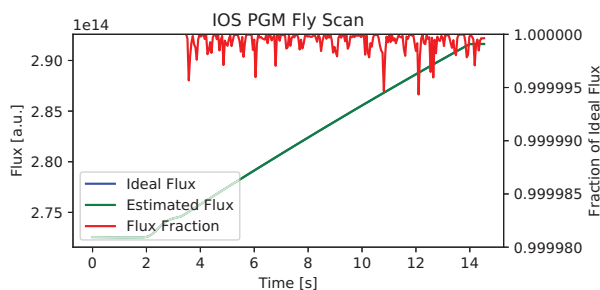

Figure 7: The estimated ideal flux and fractional deviation from ideal based on the monochromator following error.

(EPICS) software [6], Control System Studio (CSS) [7], and Bluesky Data Collection Framework [8]. EPICS provides Input/Output Controller (IOC) software for the Delta Tau controllers and the networking framework, CSS is used for basic device control and readback, and Bluesky is used for more complex scanning and data collection routines.

The ID and monochromator controllers operate either in an individual mode or a linked mode via the Delta Tau MACRO connection. The individual control mode is necessary when ID control is restricted to accelerator operators. The mode is selected using EPICS, which triggers a script on the Delta Tau controller to configure and toggle the MACRO link. The linked mode used for fly scanning performs kinematics of both devices on the ID controller and overrides some normal functionality on the PGM controller. Fly scans are defined with a start energy, stop energy, and speed defined in [eV/s]. Trigger outputs are independently defined with a start, stop, and step energy. Typically the energy range of the fly scan will be larger than the triggering range to allow the motors to reach a steady state over the energy range of interest. Bluesky routines manage the staging and unstaging of detectors and manage detector data and associated meta data.

motion diagnostics and programming techniques developed for the IVU controls and that the PGM will likely exhibit higher accuracy during motion once the 2-motor axes are completely decoupled and mechanical cross-talk feedback is eliminated. Currently a five volt TTL trigger is provided at user configurable uniform spacing in [eV] by a PLC program running on the controller that is evaluated at approximately 300 [Hz], depending on controller CPU load, for a virtual motor running in the coordinate system representing energy.

In order to get an idea of the variation in flux from the fly scan data shown in Fig. 6 one can use the theoretical flux for a given gap shown in Fig. 4. The harmonic width in [eV] is large compared to the ID following error. If we ignore this small effect and assume a much smaller than reality harmonic width we can estimate the change in flux from the ideal case from the following error of the monochromator, assuming that this dictates the photon energy at the end station. For this we assume gaussian spectral peaks of width 10 [eV] (which is an underestimate, but will give an over-estimated upper limit on the variation in flux from the monochromator). We obtain an off-peak correction from a gaussian factor based on the difference of ID energy and monochromator energy. The estimated fraction of the ideal flux is shown in Fig. 7 and deviates by less than 10 ppm.

CONCLUSION

A total of 8 IVU control systems have been updated for high reliability and high precision. This work is in part also preparation for ID-monochromator synchronous motion for fly scanning. The ID and PGM at IOS was the first ID beamline at NSLSII to be configured for these type of fly scans and estimates of precision of motion and deviation from ideal flux have been attained.

ACKNOWLEDGMENTS

CONTROL LAYERS

Control of the ID and monochromator is performed using Experimental Physics and Industrial Control System

REFERENCES

[1] NSLS-II ID Working Group, private communication

[2] J. Krempasky, U. Flechsig, T. Korhonen, D. Zimoch, Ch. Quitmann, and F. Nolting, "Synchronized monochromator and insertion device energy scans at SLS," *AIP Conference Proceedings*, vol. 1234, no. 1, Jun. 2010. doi:10.1063/1.3463307

[3] Open Source Code for Advanced Radiation Simulation, https://oscars.bnl.gov

[4] M. Musardo, D. A. Harder, C. A. Kitegi, and T. Tanabe, "Magnetic Measurements of the NSLS-II Insertion Devices", in *Proc. IPAC'15*, Richmond, VA, USA, May 2015, pp. 1693–1695. doi:10.18429/JACoW-IPAC2015-TUPJE037

[5] M. Musardo *et al.*, "Recent Magnetic Measurement Activities at NSLS-II Insertion Device Laboratory", in *Proc. IPAC'16*, Busan, Korea, May 2016, pp. 4063–4065. doi:10.18429/JACoW-IPAC2016-THPOW052

[6] EPICS Software, https://epics-controls.org/

[7] Control System Studio, http://controlsystemstudio.org/

[8] Bluesky Data Collection Framework, https://nsls-ii.github.io/bluesky/